

Hyperbolic Fringe Signal for Twin Impurity Quasiparticle Interference

Peize Ding^{1,2,3,*}, Tilman Schwemmer¹, Ching Hua Lee^{4,5}, Xianxin Wu^{6,†}, and Ronny Thomale^{1,‡}

¹*Institute for Theoretical Physics, University of Würzburg, Am Hubland, D-97074 Würzburg, Germany*


²*School of the Gifted Young, University of Science and Technology of China, Hefei 230026, China*

³*Department of Physics, Columbia University, New York, New York 10027, USA*

⁴*Department of Physics, National University of Singapore, Singapore, 117542*

⁵*Joint School of National University of Singapore and Tianjin University, International Campus of Tianjin University, Binhai New City, Fuzhou 350207, China*

⁶*CAS Key Laboratory of Theoretical Physics, Institute of Theoretical Physics, Chinese Academy of Sciences, Beijing 100190, China*

 (Received 5 July 2022; revised 31 October 2022; accepted 17 May 2023; published 21 June 2023)

We study the quasiparticle interference (QPI) pattern emanating from a pair of adjacent impurities on the surface of a gapped superconductor (SC). We find that hyperbolic fringes (HFs) in the QPI signal can appear due to the loop contribution of the two-impurity scattering, where the locations of the two impurities are the hyperbolic focus points. For a single pocket Fermiology, a HF pattern signals chiral SC order for nonmagnetic impurities and requires magnetic impurities for a nonchiral SC. For a multipocket scenario, a sign-changing order parameter such as an s_{\pm} wave likewise yields a HF signature. We discuss twin impurity QPI as a new tool to complement the analysis of superconducting order from local spectroscopy.

DOI: [10.1103/PhysRevLett.130.256001](https://doi.org/10.1103/PhysRevLett.130.256001)

Introduction.—Quasiparticle interference (QPI) around impurities, which can be probed through a scanning tunneling microscopy (STM) measurement, has acquired a pivotal role in exploring the properties of unconventional electronic states of matter including high- T_c superconductors (SCs) [1–8] and topological insulators (TIs) [9,10]. For the SC, the local density of states (LDOS) modulation patterns not only reflect principal features of electronic dispersion and pairing symmetries [1,11–13], but are also sensitive to sign changes in the SC order parameter [3–5] as well as to time-reversal symmetry [10,14]. In addition to QPI patterns arising from a single impurity, the LDOS distribution and possible bound states due to the presence of multiple impurities have been studied in a variety of systems [15–20].

The QPI pattern's phase sensitivity renders it preeminently suited to resolve intricate properties of an unconventional SC state of matter. At present, the evidence on the nature of unconventional pairing symmetry of several material classes is still incomplete. This includes candidates for the chiral SC order such as strontium ruthenate [21], Na-doped cobaltates [22] or, more lately, Sn/Si heterostructures [23] and kagome metals [24]. Likewise, additional ways to track the sign-changing nature of extended s -wave order, as suspected for many iron pnictide families, are highly sought after [25].

In this Letter, we propose a hyperbolic fringe (HF) signal fingerprint found in the QPI pattern of two adjacent impurities deposited on a gapped SC, which we coin *twin QPI*. We find that through the HF signal, the twin QPI pattern allows us to retrieve information beyond the single

impurity case, and thus to draw conclusions on the either chiral or multipocket sign changing nature of the SC order parameter.

Minimal model.—In order to complement the numerical analysis with an analytically tractable limit to showcase the mathematical structure of the HF pattern, we initially constrain ourselves to the simplest Bardeen-Cooper-Schrieffer (BCS) Hamiltonian for a single electronic band with nearest neighbor hybridization on a square lattice $\epsilon_{\mathbf{k}} = -2t(\cos k_x + \cos k_y) - \mu$:

$$H = \sum_{\mathbf{k}s} \epsilon_{\mathbf{k}} c_{\mathbf{k}s}^{\dagger} c_{\mathbf{k}s} + \sum_{\mathbf{k}} (\Delta_{\mathbf{k}} c_{\mathbf{k}\uparrow}^{\dagger} c_{-\mathbf{k}\downarrow}^{\dagger} + \text{H.c.}), \quad (1)$$

where we set the hopping parameter $t = 1$ and the lattice spacing $a = 1$. Initially, we assume the chemical potential to be located at fillings where the Fermi surface (FS) is approximately circular [Fig. 2(a) red line]. The presence of impurity scattering is modeled by

$$H_{NM(M)}^{\text{imp}} = U_0 \sum_{\mathbf{r}} \sum_n \delta_{\mathbf{r},\mathbf{r}_n} (c_{\mathbf{r}\uparrow}^{\dagger} c_{\mathbf{r}\uparrow} \pm c_{\mathbf{r}\downarrow}^{\dagger} c_{\mathbf{r}\downarrow}), \quad (2)$$

where \mathbf{r}_n denotes the location of impurities, U_0 is the impurity coupling strength, and the $+$ ($-$) sign corresponds to nonmagnetic (magnetic), impurities. The QPI pattern observed by a STM measurement is related to the LDOS distribution $N(\mathbf{r}, \omega)$, where we recast ω as the frequency bias of the STM tip. It reads

$$N(\mathbf{r}, \omega) = -\frac{1}{\pi} \text{ImTr} \left[\frac{\hat{1} + \hat{\tau}_z}{2} \mathbf{G}(\mathbf{r}, \mathbf{r}, \omega + i\eta) \right], \quad (3)$$

where \mathbf{G} denotes the Nambu Green's function, with the four-component spinor operator given by $(c_{\mathbf{k},\uparrow}^\dagger, c_{-\mathbf{k},\downarrow}^\dagger, c_{-\mathbf{k},\downarrow}, c_{\mathbf{k},\uparrow})$ in momentum space. $\vec{\tau} = (\tau_x, \tau_y, \tau_z)$ denotes the Pauli

matrix vector in particle-hole space, and η denotes an infinitesimal positive number regulator. In the absence of impurities, the Green's function is given by

$$\mathbf{G}_0(\mathbf{r}, \omega) \equiv \begin{pmatrix} G_0(\mathbf{r}, \omega) & 0 & F_0(\mathbf{r}, \omega) & 0 \\ 0 & G_0(\mathbf{r}, \omega) & 0 & F_0(\mathbf{r}, \omega) \\ \tilde{F}_0(\mathbf{r}, \omega) & 0 & -G_0(\mathbf{r}, -\omega) & 0 \\ 0 & \tilde{F}_0(\mathbf{r}, \omega) & 0 & -G_0(\mathbf{r}, -\omega) \end{pmatrix}, \quad (4)$$

where

$$\begin{pmatrix} G_0(\mathbf{r}, \omega) \\ F_0(\mathbf{r}, \omega) \\ \tilde{F}_0(\mathbf{r}, \omega) \end{pmatrix} = \frac{1}{\mathcal{S}} \sum_{\mathbf{k}} \frac{e^{i\mathbf{k}\cdot\mathbf{r}}}{\omega^2 - \varepsilon_{\mathbf{k}}^2 - \Delta_{\mathbf{k}}^2 + i0^+} \begin{pmatrix} \omega + \varepsilon_{\mathbf{k}} \\ \Delta_{\mathbf{k}} \\ \Delta_{\mathbf{k}}^* \end{pmatrix}, \quad (5)$$

and \mathcal{S} is the area of the sample. In the presence of impurities, the full Green's function is expanded with respect to U_0 to obtain the infinite series

$$\begin{aligned} \mathbf{G}(\mathbf{r}, \mathbf{r}') &= \mathbf{G}_0(\mathbf{r} - \mathbf{r}') + \sum_{\mathbf{r}''} \mathbf{G}_0(\mathbf{r} - \mathbf{r}'') U(\mathbf{r}'') \mathbf{G}_0(\mathbf{r}'' - \mathbf{r}') \\ &+ \sum_{\mathbf{r}''} \mathbf{G}_0(\mathbf{r} - \mathbf{r}'') U(\mathbf{r}'') \\ &\times \mathbf{G}_0(\mathbf{r}'' - \mathbf{r}''') U(\mathbf{r}''') \mathbf{G}_0(\mathbf{r}''' - \mathbf{r}') + \dots, \quad (6) \end{aligned}$$

where $U(\mathbf{r}) = U \sum_n \delta_{\mathbf{r}, \mathbf{r}_n}$ with $U = U_0 \tau_z$ for nonmagnetic and $U = U_0 \sigma_z$ [$\vec{\sigma} = (\sigma_x, \sigma_y, \sigma_z)$ is the Pauli matrix vector in spin space] for magnetic impurities. Note that for scattering around a pair of magnetic impurities, unless otherwise stated, we assume that their magnetic moments are aligned.

Hyperbolic fringes in twin QPI.—Assume two impurities to be located at \mathbf{r}_1 and \mathbf{r}_2 . While there are infinitely many terms, we can separate them into two classes. The first contains all processes from \mathbf{r} to \mathbf{r}_1 (\mathbf{r}_2), and after possible multibouncing, back to \mathbf{r} from \mathbf{r}_1 (\mathbf{r}_2). We call this class *single contribution*. The other part contains processes from \mathbf{r} to \mathbf{r}_1 (\mathbf{r}_2), and after possible multibouncing, back to \mathbf{r}

from \mathbf{r}_2 (\mathbf{r}_1), which we call *loop contribution*. In each class, the terms are summed up as a geometric series. The multibouncing processes at one impurity only renormalize U according to $U' = [\hat{1} - U\mathbf{G}_0(0)]^{-1}U$. Summing up all the multibouncing processes between two impurities yields a second step renormalization of U' according to $U'' = [\hat{1} - U'\mathbf{G}_0(\mathbf{r}_1 - \mathbf{r}_2)U'\mathbf{G}_0(\mathbf{r}_2 - \mathbf{r}_1)]^{-1}U'$. We get

$$\mathbf{G}(\mathbf{r}, \mathbf{r}) - \mathbf{G}_0(0) = \mathbf{G}_0(\mathbf{r} - \mathbf{r}_1) U'' \mathbf{G}_0(\mathbf{r}_1 - \mathbf{r}) + (1 \leftrightarrow 2) \quad (7)$$

$$+ \mathbf{G}_0(\mathbf{r} - \mathbf{r}_2) U' \mathbf{G}_0(\mathbf{r}_2 - \mathbf{r}_1) U'' \mathbf{G}_0(\mathbf{r}_1 - \mathbf{r}) + (1 \leftrightarrow 2), \quad (8)$$

where the lines (7) and (8) denote single and loop contribution, respectively. We assume a gapped single-pocket s -wave SC $\Delta_{\mathbf{k}}^s = \Delta$ and an electronic filling close to the band edge such that we obtain an approximately circular Fermi surface [Fig. 2(a) red line]. This allows us to gain an analytical grasp on $\mathbf{G}_0(\mathbf{r}, \omega)$. Setting $k_F = 1$, we find [26]

$$G_0(\mathbf{r}) \sim r^{-1/2} \left[\sin r - \frac{i\omega}{\omega'} \cos r \right], \quad (9)$$

and

$$F_0^s(\mathbf{r}) = \tilde{F}_0^s(\mathbf{r}) \sim \frac{i\Delta}{\omega'} r^{-1/2} \cos r, \quad (10)$$

where $r \equiv |\mathbf{r}|$ and $\omega' \equiv \sqrt{\omega^2 - \Delta^2}$. To second order in U_0 , we find from Eqs. (4), (9), and (10)

$$N^{\text{loop},s}(\mathbf{r}) \sim (r_1 r_2 d)^{-1/2} \begin{cases} \cos(r_1 + r_2 + d), & NM \\ \cos(r_1 + r_2 + d) + \frac{4\Delta^2}{\omega'^2} \cos r_1 \cos r_2 \cos d, & M \end{cases} \quad (11)$$

where $r_1 = |\mathbf{r} - \mathbf{r}_1|$, $r_2 = |\mathbf{r} - \mathbf{r}_2|$, and d denotes the distance between the two impurities. The nonmagnetic (NM) expression explains the elliptical oscillations in Fig. 1(b) (we perform numerical simulations based on

the full tight-binding Hamiltonian, details in [29]), where the constant contours are $r_1 + r_2 = C$, with C given by some constant. In contrast, the magnetic (M) expression is the summation of oscillations of $r_1 + r_2$ and that of $r_1 - r_2$.

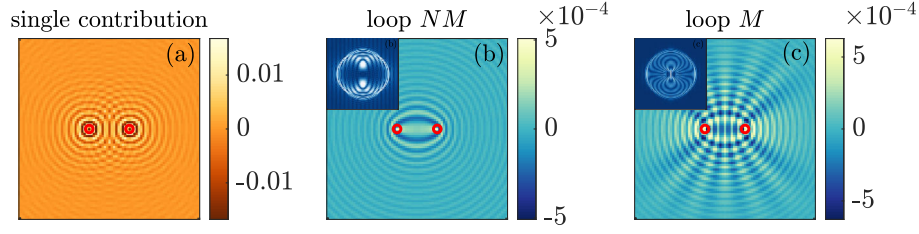


FIG. 1. Twin impurity QPI for a single-pocket s -wave SC ($\mu = -3$, $\Delta = 0.1$, $\omega = 1.1\Delta$, $d = 18$) in real space. Note that the shown LDOS is measured in units of $(ta^2)^{-1}$ and thus is dimensionless for our choice of $a = 1$ and $t = 1$. (a) Single impurity contribution to the QPI pattern. (b) Loop contribution to QPI for nonmagnetic (NM) twin impurities. (c) Loop contribution to QPI for magnetic (M) twin impurities. The insets show the Fourier transformation of the patterns. A hyperbolic fringe (HF) pattern emerges on top of the elliptical fringe background.

As $r_1 - r_2 = C$ is the very definition of a hyperbola, a HF appears in Fig. 1(c) on top of the elliptical oscillations. The emergence of a HF is attributed to the loop quasiparticle scattering. This pattern in the LDOS remains qualitatively unchanged upon including higher-order scattering terms, as described in detail in the Supplemental Material (SM). When $\omega \gg \Delta$, the superconducting coherence is lost on the equal energy contour, and we recover the nonmagnetic results [Eq. (11)] which is the same as that in a metal. Also, note that the elliptical and hyperbolic fringes exhibit manifestly different Fourier transformations [(b) and (c) inset], which we detailed in the SM.

Chiral SC.—While some aspects of the HF signal for the s -wave minimal model above carry over to chiral pairing symmetries, the twin QPI pattern of a chiral SC already exhibits a HF signal for nonmagnetic impurities. Picking $\Delta_{\mathbf{k}}^p = \Delta(\sin k_x + i \sin k_y)$ for illustration, we find G_0 according to Eq. (9) along with

$$F_0^p(\mathbf{r}) = [\tilde{F}_0^p(\mathbf{r})]^* \sim \frac{i\tilde{\Delta}}{\omega'} r^{-1/2} \sin r e^{i\theta}, \quad (12)$$

where θ is the polar angle of \mathbf{r} . This gives a loop contribution to the LDOS according to

$$N_p^{\text{loop}}(\mathbf{r}) \sim (r_1 r_2 d)^{-1/2} \times \left\{ \begin{aligned} &\cos(r_1 + r_2 + d) \\ &+ \frac{\Delta^2}{\omega'^2} [\sin r_1 \sin r_2 \cos d \cos(\theta_1 - \theta_2) \\ &+ \cos r_1 \cos r_2 \cos d \\ &\pm (\cos r_1 \sin r_2 \sin d \cos \theta_2 \\ &- \sin r_1 \cos r_2 \sin d \cos \theta_1)] \end{aligned} \right\}, \quad (13)$$

where θ_1 and θ_2 denote the polar angle of $\mathbf{r} - \mathbf{r}_1$ and $\mathbf{r} - \mathbf{r}_2$, respectively, and $+$ ($-$) corresponds to NM (M) impurities. According to trigonometric transformations, we immediately recognize that Eq. (13) is also the summation of the oscillations of $r_1 + r_2$ and of $r_1 - r_2$, albeit the amplitude is further modulated by terms related to the polar angles θ_1 and θ_2 . That is why we also see a HF on top of elliptical fringes in Fig. 2(b). We employ Eq. (13) in Fig. 2(d) to compare our analytical approximation against the numerical calculation in Fig. 2(b), which shows good agreement. In contrast to the uniform s -wave pairing, here the two scattering processes $\mathbf{r} \rightarrow \mathbf{r}_1 \rightarrow \mathbf{r}_2 \rightarrow \mathbf{r}$ and $\mathbf{r} \rightarrow \mathbf{r}_2 \rightarrow \mathbf{r}_1 \rightarrow \mathbf{r}$, which are time-reversed to each other, can also interfere to generate the HF, as the superconducting gaps acquire different winding phases on the two paths.

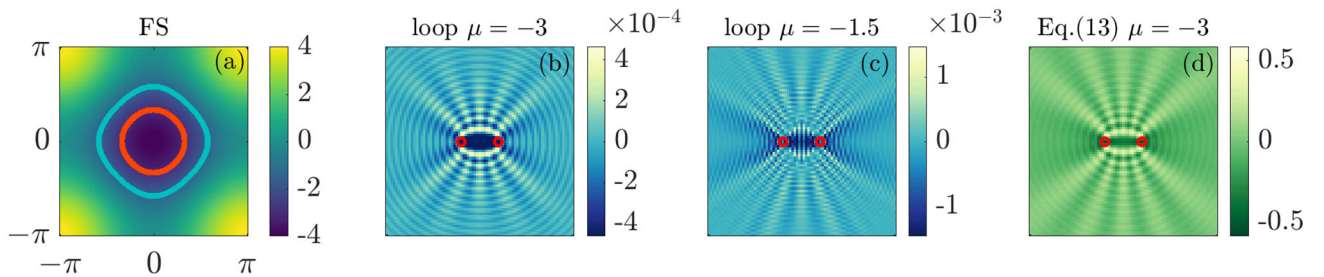


FIG. 2. Twin impurity QPI for a single-pocket chiral SC ($\Delta = 0.05$, $\omega = 1.1\Delta$, $d = 16$). (a) Band dispersion $\epsilon(\mathbf{k}) = -2(\cos k_x + \cos k_y)$ (denoted by color) and the FS at $\mu = -3$ (red line) and $\mu = -1.5$ (blue line) in the first Brillouin zone. (b),(c) Twin nonmagnetic impurity loop contribution for $p + ip$ -wave pairing with $\mu = -3$ and $\mu = -1.5$. (d) A plot of our analytical expression [Eq. (13)] for the loop contribution (in arbitrary unit) on a 81×81 real space lattice with $\mu = -3$ shows the expected agreement with the corresponding numerical results presented in panel (b).

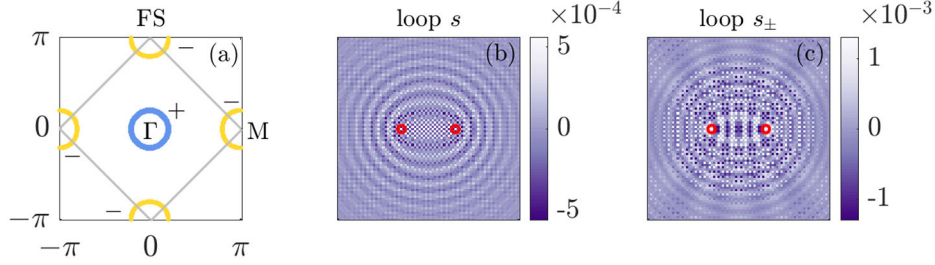


FIG. 3. Twin impurity QPI for a multipocket s_{\pm} -wave SC ($\omega = 0.3232$, $d = 24$). (a) FS of the “ c ” (denoted by yellow line) and the “ d ” (denoted by blue line) electron bands of a two-band model. + (–) denote the sign of the gap for s_{\pm} -wave pairing. (b) Loop contribution from two nonmagnetic impurities for conventional on-site s -wave pairing around two nonmagnetic impurities. (c) Loop contribution as in (b) for s_{\pm} -wave pairing.

This interference is reflected in the $\cos(\theta_1 - \theta_2)$ term in Eq. (13). We further study the HF signal for a $d + id$ -wave SC and find the overall pattern to be similar to that of the $p + ip$ -wave case (see SM). The crucial difference is that the interference pattern in the region between two impurity sites for the $d + id$ -wave pairing is not uniform but stripelike, which is attributed to the distinct phase winding of two SC orders and can be explained from their detailed analytic form (details in SM). For magnetic impurities, the interference patterns are similar, as detailed in the SM.

Note that for our analytical expressions Eqs. (11) and (13) we have assumed $\eta \rightarrow 0^+$, while in numerical calculations η has to take a nonzero value (which we have chosen as $\eta = 5 \times 10^{-3}$). Having a nonzero η regulator just amounts to setting $\omega \rightarrow \omega + i\eta$ in Eqs. (9), (10), and (12), and does not affect the main features of the LDOS distribution. Departing from the band edge limit where we can compare against our analytical solution, we find that the numerical HF signature prevails even for noncircular Fermi surfaces [Fig. 2(c)]. This allows us to conjecture that the HF pattern is a generic signal for twin-impurity QPI patterns of chiral SCs, where the HF signal dependence on the chemical potential is further detailed in [26].

s_{\pm} wave in multipocket systems.—Multipocket Fermiologies can qualitatively differ from single-pocket systems. In particular, with respect to gapped SCs, multipocket systems can exhibit s_{\pm} -wave unconventional pairing where the gap function takes opposite signs on different Fermi pockets [4]. We start from a two-band model for iron-based SC ([5])

$$H = \sum_{\mathbf{k}, \sigma} (\epsilon_{\mathbf{k}}^c c_{\mathbf{k}, \sigma}^{\dagger} c_{\mathbf{k}, \sigma} + \epsilon_{\mathbf{k}}^d d_{\mathbf{k}, \sigma}^{\dagger} d_{\mathbf{k}, \sigma}) + \sum_{\mathbf{k}} [\Delta_{\mathbf{k}} (c_{\mathbf{k}, \uparrow} c_{-\mathbf{k}, \downarrow} + d_{\mathbf{k}, \uparrow} d_{-\mathbf{k}, \downarrow}) + \text{H.c.}] \quad (14)$$

Here, “ c ” and “ d ” label the two electron bands describing an electronlike FS centered at the M point in the folded Brillouin zone [or $(\pi, 0)/(0, \pi)$ for the unfolded zone [30]] and a holelike FS at the Γ point. It reads

$$\epsilon_{\mathbf{k}}^c = 2t[\cos(k_x + k_y) + \cos(k_x - k_y)] - \mu_c, \quad (15)$$

$$\epsilon_{\mathbf{k}}^d = 2t(\cos k_x + \cos k_y) - \mu_d, \quad (16)$$

where we choose $\mu_c = -3.2$ and $\mu_d = 3.6$ [Fig. 3(a)]. It turns out that s_{\pm} -wave order, as opposed to conventional s -wave order without a sign-changing order parameter, exhibits a HF signal for any kind of impurity. Consider two types of s -wave pairing:

$$\Delta_{\mathbf{k}} = \begin{cases} \Delta_s, & s \text{ wave} \\ \Delta_{s_{\pm}} \cos k_x \cos k_y, & s_{\pm} \text{ wave} \end{cases} \quad (17)$$

where $t = 1$, $\Delta_s = 0.32$, and $\Delta_{s_{\pm}} = 0.4$. The extended s -wave pairing gives the close gap magnitude but takes opposite signs on the FSs around the Γ and M points. The formalism laid out for the single pocket case readily generalizes to the two-band model by recognizing $\mathbf{G}_0(\mathbf{r}) = \mathbf{G}_0^c(\mathbf{r}) + \mathbf{G}_0^d(\mathbf{r})$, where $\mathbf{G}_0^c(\mathbf{r})$ and $\mathbf{G}_0^d(\mathbf{r})$ are defined via Eq. (4) (the unfolded Brillouin zone is used to perform the summation in the Fourier transformation) and Eqs. (15)–(17). In Figs. 3(b) and 3(c), we show the loop contribution in the LDOS distribution of the two-band SC around two nonmagnetic impurities for conventional s -wave pairing and unconventional s_{\pm} -wave pairing, respectively. For Fig. 3(c), a uniform gap ($\tilde{\Delta} = 0.32$) with opposite sign on the two electron bands is used in the underlying calculation in order to reduce the gap anisotropy. Similar to our previous results for conventional s -wave pairing on a single pocket, the loop contribution results in elliptical fringes. In addition, however, an extended s_{\pm} -wave SC order parameter gives rise to the emergence of a HF signal on top of the ellipses. We note that the emergence of a HF is due to the fact that a sign-reversing scattering at a nonmagnetic impurity is mathematically equivalent to a sign-preserving scattering at a magnetic impurity. As we have shown for single-pocket s -wave SC, the latter case can generate a HF. The “mosaic” like feature (zigzag between neighboring sites) is due to the FS of the electronlike band centering at the M point. Since the FS of the two band model is well approximated

by circles, the formulas Eqs. (8)–(10) carry over to the two-band case and analytically explain the HF signal difference between conventional and unconventional s -wave pairing [26]. The latter distinguishability only holds for nonmagnetic impurities, as magnetic impurities imply a HF pattern in both cases. Our findings for the two-pocket case with sign changing should generalize to the generic multipocket case with a sign-changing gap function on individual pockets.

Experimental detectability.—The loop contribution is generally smaller than the single contribution according to $N^{\text{loop}}/N^{\text{single}} \sim (k_F d)^{-1/2} U_0/t$ for nonmagnetic impurities. Thus, it is crucial to isolate the loop contribution in STM measurements from the single contribution background, a procedure for which we provide two proposals. The first option involves measuring the LDOS around a single impurity before measuring close to twin impurities. By subtracting the single-impurity contribution from the full contribution, the loop contribution can be isolated. Our second proposal is specifically designed for magnetic impurities, where two measurements are made with the twin impurities with antialigned and aligned magnetic moments. While this change does not affect the individual contributions (second order), the loop signal changes sign between the configurations. Taking the difference between the two signals thus significantly suppresses the single contribution and singles out the loop contribution. In the SM, we provide detailed simulations demonstrating the effectiveness of these proposals. In the measurements, such twin impurities might be fabricated through STM atomic manipulation [31], which would further allow us to explore the evolution of the HF pattern as a function of the distance between twin impurities. A simple proof-of-principle experiment for our predicted HF pattern appears to be a conventional s -wave superconductor with a clean surface and highly adjustable magnetic impurities on top of it. A good candidate is NbSe₂, which can be grown by molecular beam epitaxy yielding clean surfaces [32] required for quasiparticle interference experiments [33]. Moreover, with their s_{\pm} -wave pairing, it is also promising to examine the HF signal in iron-based superconductors such as LiFeAs [34,35].

Conclusion and outlook.—The hyperbolic fringe pattern from twin impurity QPI provides a complementary approach of detecting phase information associated with the SC order. While conventional pairing necessitates magnetic twin impurities to generate a HF signal, chiral SC and s_{\pm} -wave multipocket SC already exhibit a HF signal for nonmagnetic impurities. Upon closer inspection of the principal underlying mathematical structure, it is apparent that the HF signal is not special to the SC, but can potentially appear in entirely different contexts such as topological insulators (TIs). For instance, the Qi-Wu-Zhang model on a two-dimensional lattice [36] for time-reversal symmetry breaking TIs exhibits a k -space Hamiltonian that

has the same form as a chiral p -wave SC. It is hence plausible that the HF signature of twin impurities should also appear in the loop contribution to the TI LDOS distribution in the topologically nontrivial regime. For other TIs and topological materials such as graphene, the QPI pattern on the surface around twin impurities presents itself as a valuable perspective for future study.

R. T. thanks his mentor and friend Shoucheng Zhang for a discussion which has provided the inspiration for this project. This work is funded by the Deutsche Forschungsgemeinschaft (DFG, German Research Foundation) through Project-ID 258499086–SFB 1170 and through the Würzburg-Dresden Cluster of Excellence on Complexity and Topology in Quantum Matter—ct.qmat Project-ID 390858490—EXC 2147. This work is also supported by the National Natural Science Foundation of China (Grant No. 12047503) and the Singapore National Research Foundation QEP grant (Grant No. NRF2021-QEP2-02-P09). Numerical calculations in this work were performed on the HPC Cluster of ITP-CAS.

*pd2714@columbia.edu

†xxwu@itp.ac.cn

‡rthomale@physik.uni-wuerzburg.de

- [1] J. M. Byers, M. E. Flatté, and D. J. Scalapino, *Phys. Rev. Lett.* **71**, 3363 (1993).
- [2] J. E. Hoffman, E. W. Hudson, K. M. Lang, V. Madhavan, H. Eisaki, S. Uchida, and J. C. Davis, *Science* **295**, 466 (2002).
- [3] Q.-H. Wang and D.-H. Lee, *Phys. Rev. B* **67**, 020511(R) (2003).
- [4] T. Hanaguri, S. Niitaka, K. Kuroki, and H. Takagi, *Science* **328**, 474 (2010).
- [5] S. Sykora and P. Coleman, *Phys. Rev. B* **84**, 054501 (2011).
- [6] H. Zheng and M. Z. Hasan, *Adv. Phys.* **3**, 1466661 (2018).
- [7] A. Akbari, J. Knolle, I. Eremin, and R. Moessner, *Phys. Rev. B* **82**, 224506 (2010).
- [8] C. Bena, *C. R. Phys.* **17**, 302 (2016).
- [9] P. Roushan, J. Seo, C. V. Parker, Y. S. Hor, D. Hsieh, D. Qian, A. Richardella, M. Z. Hasan, R. J. Cava, and A. Yazdani, *Nature (London)* **460**, 1106 (2009).
- [10] W.-C. Lee, C. Wu, D. P. Arovas, and S.-C. Zhang, *Phys. Rev. B* **80**, 245439 (2009).
- [11] A. V. Balatsky, I. Vekhter, and J.-X. Zhu, *Rev. Mod. Phys.* **78**, 373 (2006).
- [12] L. Yu, *Acta Phys. Sin.* **21**, 75 (1965).10.7498/aps.21.75
- [13] M. Mashkoori, K. Björnson, and A. M. Black-Schaffer, *Sci. Rep.* **7**, 44107 (2017).
- [14] R. Queiroz and A. Stern, *Phys. Rev. Lett.* **121**, 176401 (2018).
- [15] M. E. Flatté and D. E. Reynolds, *Phys. Rev. B* **61**, 14810 (2000).
- [16] D. K. Morr and N. A. Stavropoulos, *Phys. Rev. B* **67**, 020502(R) (2003).

- [17] C. H. Choi, J. Korean Phys. Soc. **44**, 355 (2004), <https://www.jkps.or.kr/journal/view.html?uid=5973&vmd=Full>.
- [18] L. Zhu, W. A. Atkinson, and P. J. Hirschfeld, *Phys. Rev. B* **67**, 094508 (2003).
- [19] A. Cano and I. Paul, *Phys. Rev. B* **80**, 153401 (2009).
- [20] J. Ortuzar, S. Trivini, M. Alvarado, M. Rouco, J. Zaldivar, A. L. Yeyati, J. I. Pascual, and F. S. Bergeret, *Phys. Rev. B* **105**, 245403 (2022).
- [21] A. Pustogow, Y. Luo, A. Chronister, Y. S. Su, D. A. Sokolov, F. Jerzembeck, A. P. Mackenzie, C. W. Hicks, N. Kikugawa, S. Raghu, E. D. Bauer, and S. E. Brown, *Nature (London)* **574**, 72 (2019).
- [22] M. L. Kiesel, C. Platt, W. Hanke, and R. Thomale, *Phys. Rev. Lett.* **111**, 097001 (2013).
- [23] S. Wolf, D. Di Sante, T. Schwemmer, R. Thomale, and S. Rachel, *Phys. Rev. Lett.* **128**, 167002 (2022).
- [24] T. Neupert, M. M. Denner, J.-X. Yin, R. Thomale, and M. Z. Hasan, *Nat. Phys.* **18**, 137 (2022).
- [25] G. R. Stewart, *Rev. Mod. Phys.* **83**, 1589 (2011).
- [26] See Supplemental Material at <http://link.aps.org/supplemental/10.1103/PhysRevLett.130.256001>, including Refs. [27,28] for the derivation of the analytical formulas, experimental proposals and more.
- [27] F. Pientka, L. I. Glazman, and F. von Oppen, *Phys. Rev. B* **88**, 155420 (2013).
- [28] T. Machida, Y. Sun, S. Pyon, S. Takeda, Y. Kohsaka, T. Hanaguri, T. Sasagawa, and T. Tamegai, *Nat. Mater.* **18**, 811 (2019).
- [29] By performing Fourier transformation in the first Brillouin zone via Eq. (4), and through using Eqs. (8), (3), we obtain a numerical estimate for LDOS distribution. We focus on the regime where the energy bias of the STM tip ω is slightly above the bulk gap. The strength of impurities is chosen as the typical value $U_0 = 0.9$ (of the magnitude of hundred meV) [3]. In actual calculations, a large real space lattice is needed to achieve a high momentum resolution in the Fourier transformation. In our case, we adopt the LDOS of the central 81×81 plaquette within an 800×800 discretization. Also, η should be of the same magnitude as the numerical energy resolution, i.e., $\eta \sim \delta E$. We take $\eta = 5 \times 10^{-3}$.
- [30] H. Ding, P. Richard, K. Nakayama, K. Sugawara, T. Arakane, Y. Sekiba, A. Takayama, S. Souma, T. Sato, T. Takahashi, Z. Wang, X. Dai, Z. Fang, G. F. Chen, J. L. Luo, and N. L. Wang, *Europhys. Lett.* **83**, 47001 (2008).
- [31] S. W. Hla, *Rep. Prog. Phys.* **77**, 056502 (2014).
- [32] M. M. Ugeda, A. J. Bradley, Y. Zhang, S. Onishi, Y. Chen, W. Ruan, C. Ojeda-Aristizabal, H. Ryu, M. T. Edmonds, H.-Z. Tsai, A. Riss, S.-K. Mo, D. Lee, A. Zettl, Z. Hussain, Z.-X. Shen, and M. F. Crommie, *Nat. Phys.* **12**, 92 (2016).
- [33] C. J. Arguello, E. P. Rosenthal, E. F. Andrade, W. Jin, P. C. Yeh, N. Zaki, S. Jia, R. J. Cava, R. M. Fernandes, A. J. Millis, T. Valla, R. M. Osgood, and A. N. Pasupathy, *Phys. Rev. Lett.* **114**, 037001 (2015).
- [34] M. P. Allan, A. W. Rost, A. P. Mackenzie, Y. Xie, J. C. Davis, K. Kihou, C. H. Lee, A. Iyo, H. Eisaki, and T.-M. Chuang, *Science* **336**, 563 (2012).
- [35] C. Platt, R. Thomale, and W. Hanke, *Phys. Rev. B* **84**, 235121 (2011).
- [36] X.-L. Qi, Y.-S. Wu, and S.-C. Zhang, *Phys. Rev. B* **74**, 085308 (2006).